Ten-year global particulate mass concentration derived from space-borne CALIPSO lidar observations

Xiaojun Ma [a], Zhongwei Huang [a,b,*], Siqi Qi [a], Jianping Huang [a,b], Shuang Zhang [a], Qingqing Dong [a], Xin Wang [a]

[a] Key Laboratory for Semi-Arid Climate Change of the Ministry of Education, College of Atmospheric Sciences, Lanzhou University, Lanzhou 730000, China
[b] Collaborative Innovation Center for West Ecological Safety (CIWES), Lanzhou University, Lanzhou 730000, China

HIGHLIGHTS

- Active remote sensing can provide aerosols distribution both at daytime and nighttime, even under cloudy condition.
- A method for retrieving PM_{10} & $PM_{2.5}$ mass concentration using the latest data version from CALIPSO lidar was developed.
- Global distributions, especially diurnal variations, of PM_{10} & $PM_{2.5}$ mass concentration during 2007–2016 were investigated.
- This study can be used to validate global model simulations, and evaluate aerosol impacts on environment and ecosystem.

GRAPHICAL ABSTRACT
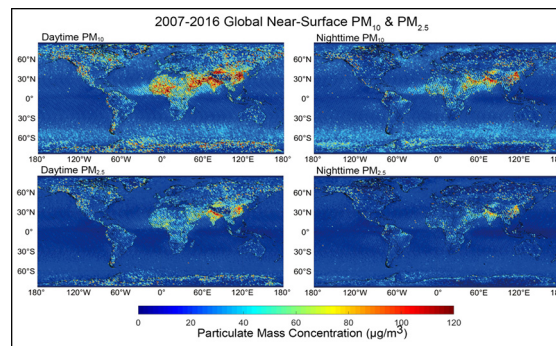
ARTICLE INFO

ABSTRACT

Passive remote sensing has been widely used in recent decades to obtain global particulate matter (PM) mass concentration at daytime and under cloud-free condition. In this study, a retrieval method was developed for providing PM (PM_{10} and $PM_{2.5}$) mass concentration both at daytime and nighttime using the latest data version (V4.10) from space-borne Cloud-Aerosol Lidar and Infrared Pathfinder Satellite Observation (CALIPSO) lidar measurements. The advantage of the method is that PM_{10} & $PM_{2.5}$ mass concentrations were obtained for seven aerosol types respectively base on active remote sensing observation at daytime and nighttime, even under cloudy condition. The results show that satellite-based PM mass concentrations are in good agreement with in-situ observations from 1602 ground monitoring sites throughout the world. Moreover, global distributions of PM_{10} and $PM_{2.5}$ mass concentration during 2007–2016 were investigated, showing that for Beijing the annual mean $PM_{2.5}$ mass concentration at nighttime is 11.31% less than those at daytime, however for London is 36.62%. It is suggested that diurnal variations in $PM_{2.5}$ mass concentration are closely related to human activities. This work provides a reliable high-resolution database for long-term particulate mass concentrations on the global scale, which is of importance to evaluate aerosol impacts on climate, environment as well as ecosystem.

© 2020 Elsevier B.V. All rights reserved.

* Corresponding author at: Key Laboratory for Semi-Arid Climate Change of the Ministry of Education, College of Atmospheric Sciences, Lanzhou University, Lanzhou 730000, China.
E-mail address: huangzhongwei@lzu.edu.cn (Z. Huang).

1. Introduction

Atmospheric particulate matter (PM) plays a significant role in the global environment and climate (Kampa and Castanas, 2008; Wilson et al., 2010; Huang et al., 2015a; Shrivastava et al., 2017; Huang et al., 2020), as well as biological processes (Ma et al., 2013). Exposure to PM with aerodynamic diameters of <2.5 μm ($PM_{2.5}$) is associated with increased cardiovascular and respiratory morbidity (Geng et al., 2015). Following uncontrolled industrial emissions and rapid global economic development, $PM_{2.5}$ mass concentrations are increasing in areas of intensive human activity (Wilson et al., 2010; Yang et al., 2017). Many previous studies have shown that aerosols can directly change the radiation balance of the earth system via reflection and scattering (Huang et al., 2007; Huang et al., 2008; Fu et al., 2009; Kato et al., 2013), and influence atmospheric radiation indirectly by changing the physical properties of clouds (Su et al., 2008; Wang et al., 2010; Li et al., 2015a, 2015b). As reported by the Intergovernmental Panel on Climate Change (IPCC, 2014) report, estimation of radiative forcing for different types of aerosols still has large uncertainty due to a lack of accurate information concerning the global spatial and temporal distribution of aerosols properties, such as concentration, components and size etc. (Huang et al., 2010).

Over the past decades, global distribution of aerosol mass concentration has been obtained based on space-borne passive and active remote sensing. As one of the most important parameters, aerosol optical depth (AOD) is widely used to determine PM concentrations in the atmosphere. By use of passive remote sensing observation, distributions of PM concentrations at daytime have been provided on the regional and/or global scale from AOD data. These data are mainly retrieved from several satellites, such as MODerate-resolution Imaging Spectroradiometer (MODIS) (Donkelaar et al., 2006; Just et al., 2015; Lin et al., 2015; Xie et al., 2015; Ghotbi et al., 2016), Multi-angle Imaging Spectroradiometer (MISR) (Geng et al., 2015) or Polarization and Anisotropy of Reflectance for Atmospheric Sciences coupled with Observations from a Lidar (PARASOL) (Xie et al., 2013). Furthermore, PM mass concentrations at night were retrieved using Visible Infrared Imaging Radiometer Suite (VIIRS) observation (Fu et al., 2018; Wang et al., 2016) with large uncertainty. To reduce the uncertainty over bright surfaces, new aerosol retrieval algorithms have been developed, including Multi-Angle Implementation of Atmospheric Correction (MAIAC) (Hu et al., 2014; van Donkelaar et al., 2016) and Deep Blue (DB) (He and Huang, 2018; Kumar et al., 2018). However, the current PM retrieval methods based on passive remote sensing still have the following main limitations: (1) lack of aerosol detection data sets suitable for both day and night; (2) cannot provide vertical structure of aerosols; (3) uncertainty over high-albedo surface areas; and (4) affected by clouds that cover 70% of Earth's surface (with optical depth > 0.1) (Stubenrauch et al., 2013).

To better investigate the impact of aerosols on global climate and environment, reliable global PM concentrations from long-term continuous observations of active remote sensing with high spatial-temporal resolutions are of great importance. Space-borne CALIPSO has provided continuous measurements of aerosols and cloud in the atmosphere on a global scale since 2006 (Omar et al., 2009; Winker et al., 2010; Huang et al., 2015b; Liu et al., 2018). As a powerful active remote sensing onboard CALIPSO, the Cloud-Aerosol lidar with Orthogonal Polarization (CALIOP) can profile the vertical distribution of aerosols and cloud with high spatial resolutions (Chen et al., 2010; Sun et al., 2015; Huang et al., 2018; Liu et al., 2018). Previous studies have introduced retrieval methods of the vertical distribution of PM mass concentrations from lidar measurements on a regional scale (Koelemeijer et al., 2006; Wang et al., 2010a; Lin et al., 2015; Li et al., 2016; Tao et al., 2016; Toth et al., 2018). And regional aerosol concentrations have been obtained from CALIPSO observations without considering aerosol types (Huang et al., 2015a, 2015b; Li et al., 2016). Moreover, deep learning technology also has been used to retrieve aerosol parameters (Chen et al., 2018; Shen et al., 2018). However, these methods didn't consider aerosol types, which may influence the accuracy of retrieval.

In this study, we retrieve global PM mass concentrations by use of the latest version (ver. 4.10) of space-borne CALIPSO lidar products. After that diurnal variations in near-surface global PM mass concentration from 2007 to 2016 are investigated. Detailed methods and observational data are introduced in Section 2; results and discussion are presented in Section 3, and conclusions are summarized in Section 4.

2. Data and methodology

2.1. CALIPSO lidar observations

CALIPSO lidar can provide three-dimensional global distributions of aerosol properties in the atmosphere with high-resolution, even over regions covered in super-thin cloud (Sun et al., 2015). It is a dual-wavelength lidar which detects backscattering signal at 1064 nm and polarization measurements at 532 nm, detail information of CALIPOSO lidar please refer to Winker et al. (2010). The latest version (ver. 4.10) of CALIPSO products Level 2 released in November 2016 was used in this study. Compared with the previous version, the new version of data has three important improvements including: (1) new geographic data; (2) redefining aerosol classification rules; (3) updating lidar ratio of all types of aerosols (Omar et al., 2018). Therefore, it is proved that the reliability of the latest version was greatly improved (Kar et al., 2018; Kim et al., 2018). In the latest version there were seven types of aerosol: clean marine (CM), pure dust (DU), polluted dust (PD), polluted continental and smoke (PC/SM), clean continental (CC), elevated smoke (ES) and dusty marine (DM). An important difference is that marine aerosol combining with dust have been frequently found over the ocean (Aller et al., 2017). So DM is defined as an important new aerosol type, however they usually was misidentified as polluted dust in the previous version (Kim et al., 2018). Vertical profiles of the aerosol extinction coefficient (α) at 532 nm and classification of aerosol types is included in the product (Omar et al., 2009).

In this study, vertical profiles of the α for seven aerosol types from CALIPSO observation during 2007–2016 was used to retrieve PM mass concentration. The vertical resolution of α profiles used was 60 m below 8.2 km. To avoid the effects of strong turbulence near the ground, the averaged α between 120 m to 180 m above ground level (AGL) which were closest to the ground was used to approximate PM mass concentration and compare with results from in-situ ground-based measurements. The Cloud and Aerosol Discrimination (CAD) algorithm score and the Extinction Quality Control (Extinction_QC_532) flag were applied to ensure data quality. In this study, we collected α with CAD value between −100 and − 20, and Extinction_QC_532 value of 0, 1, 2, 16 or 18 (Toth et al., 2018). In addition, the relative humidity profiles were provided from the MERRA-2 data product by GMAO Data Assimilation System (https://wwwcalipso.larc.nasa.gov/resources/calipso_users_guide/data_summaries/profile_data_v410.php#relative_humidity).

Table 1
Lookup table for the key parameters of seven types of aerosol used in this study.

Aerosol types	R_{eff} (μm)	Q_{ex}	ρ (g·cm^{-3})
CM	0.86	2.31	1.76
DU	0.88	2.26	1.80
PC/SM	0.46	3.48	2.00
CC	0.88	2.73	1.78
PD	0.54	2.89	1.50
ES	0.40	3.60	1.10
DM	0.61	2.92	1.79

CALIPSO Lidar Data

AERONET Data

R$_{eff, i}$

α

Aerosol Types
1: CM = Clean Marine
2: DU = Dust
3: PC/SM = Polluted Continental/Smoke
4: CC = Clean Continental
5: PD = Polluted Dust
6: EM = Elevated Smoke
7: DM = Dusty Marine

Mie Model

f(RH)

α_{dry}

$$Q_{ex} = \frac{2}{x^2} \sum_{n=1}^{\infty} (2n+1)\,\mathrm{Re}(a_n + b_n)$$

$$x = \frac{2\pi r}{\lambda}$$

Q$_{ex, i}$

$$PM_{+\infty, j} = \frac{4 \cdot R_{eff,j} \cdot \rho_j \cdot \alpha_{dry} \cdot C_{i,j}}{3 \cdot Q_{ex,j}}$$

ρ_i

PM$_{10}$ & PM$_{2.5}$
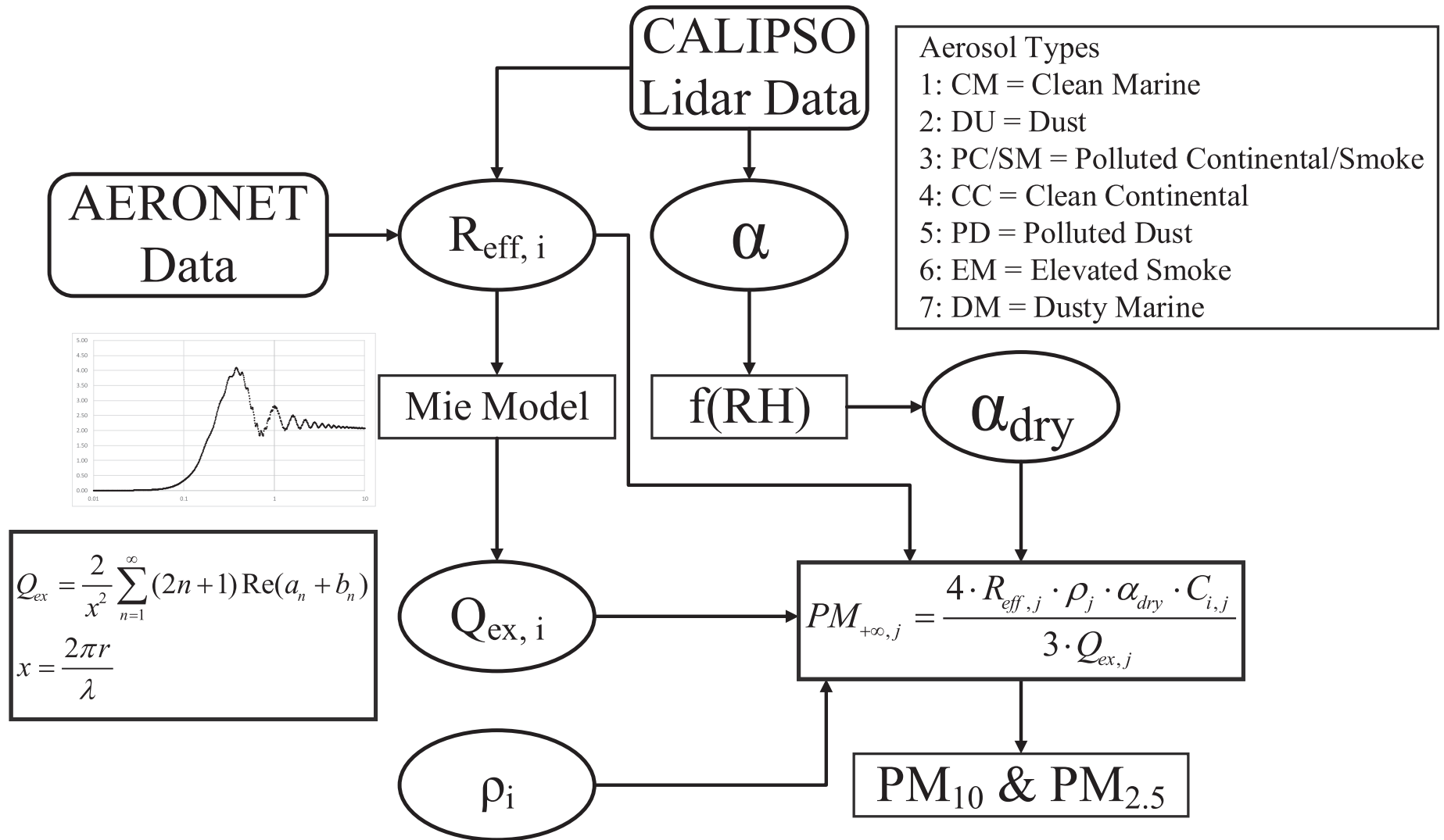
Fig. 1. A flowchart for retrieving PM$_{10}$ and PM$_{2.5}$ mass concentrations from CALIPSO lidar measurements.
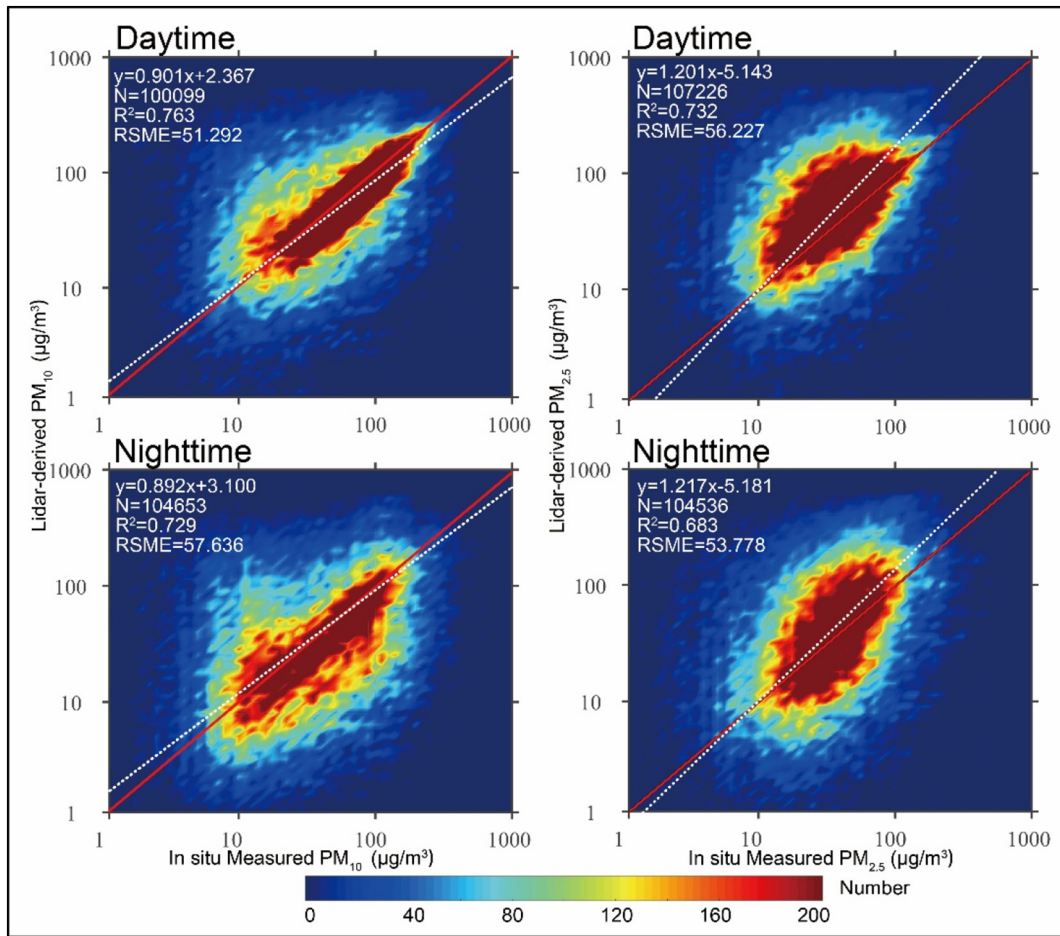
Fig. 2. Comparison of lidar-retrieved PM$_{10}$ (left) and PM$_{2.5}$ (right) in day and night with in situ measurements at 1602 ground monitoring sites throughout the world during 2007 to 2016.

2.2. Ground-based measurements

Aerosol Robotic Network (AERONET) is an internationally federated global ground-based aerosol monitoring network comprising >500 sites. AERONET sun-photometers can measure sun direct irradiances on multiple discrete channels within the spectral range of 340–1640 nm (Holben et al., 1998; Holben et al., 2001; Bi et al., 2014). In this study, as one of the key parameters for our retrieval method, the effective radii (R$_{eff}$) of seven types of aerosol were obtained from the AERONET level 2.0 inversion product. The available aerosol optical parameters from AERONET include optical thickness, particle spectrum distribution, single scattering albedo etc. The size range of aerosol observed by AERONET is 0.05–15 μm. The particle number concentration distribution is obtained by Eq. (1), and the effective radius is defined as Eq. (2).

$$\frac{dV(r)}{d \ln r} = V(r)\frac{dN(r)}{d \ln r} = \frac{4}{3}\pi r^3 \frac{dN(r)}{d \ln r} \qquad (1)$$

$$R_{eff} = \frac{\int_{r_{min}}^{r_{max}} r^3 \frac{dN(r)}{d \ln r} d \ln r}{\int_{r_{min}}^{r_{max}} r^2 \frac{dN(r)}{d \ln r} d \ln r} \qquad (2)$$

In addition, hourly average PM mass concentration measurements from 1602 global observation sites were used to validate lidar-derived results. These in situ measurements during 2007–2016 were collected from the official websites of sites. Detail information can be found in the supplementary material.

2.3. Retrieval method

The aerosol extinction coefficient (α) can be expressed as follows:

$$\alpha = \int \pi r^2 Q_{ex_j} n(r)dr \qquad (3)$$

where r is the actual radius of the aerosol particle in units of μm; Q$_{ex}$ is the aerosol extinction efficiency; n(r) is the number concentration distribution at different sizes of aerosols.

The mass concentration of PM can be expressed as:

$$PM_{i,j} = \int_0^i \frac{4}{3}\pi r^3 \rho_j n(r)dr \qquad (4)$$

i is the range of particle diameters, assigned a value of +∞, 10 or 2.5. PM$_{+\infty}$, also known as total suspended particulate matter (TSP), is defined as the total mass of particles in the atmosphere. PM$_{10}$ (inhalable particulate matter) is defined as particulate matter with an aerodynamic diameter of <10 μm, and PM$_{2.5}$ (fine particulate matter) is defined as particulate matter with a diameter of <2.5 μm. In this paper, PM$_{+, j}$, PM$_{10, j}$ and PM$_{2.5, j}$ means the mass concentration of PM$_{+\infty}$, PM$_{10}$ and PM$_{2.5}$ for seven types of aerosol. j is the type of aerosol classified by CALIPSO lidar and assigned a number from 1 to 7. ρ is the particle mass density in units of g·cm^{-3}.

Consequently, combine the above two equations (Eq. (4) ÷ Eq. (3)) we obtain:

$$PM_{+\infty,j} = \frac{4 \cdot R_{eff_j} \cdot \rho_j}{3 \cdot Q_{ex_j}} \cdot \alpha \tag{5}$$

$$R_{eff_j} = \frac{\int_0^i r^3 n(r) dr}{\int_0^i r^2 n(r) dr} \tag{6}$$

In this study, R_{eff_j} (Eq. 6) is the effective radii of each type of aerosols, independently provided by AERONET sun-photometer observations, and the corresponding statistical period of different sites for each type of aerosol was obtained from previous studies, as shown in Fig. 1 of Supplementary material. $Q_{ex, j}$ of seven types of aerosol are calculated by using Mie simulation (www.philiplaven.com/mieplot.htm) based on spherical particle hypothesis. Mieplot simulation has been recognized in optical research (Laven, 2004; Lock et al., 2014). Refraction indices were provided by Omar's research (Omar et al., 2009). $R_{eff\,j}$ and refraction indices were input parameters, summarized in table 2 and table 3 of Supplementary material. ρ_j of seven types of aerosol are summarized from previous published literatures, as shown in table 4 of Supplementary material.

Considering the effect of relative humidity (RH) on particles, RH correction factor (f(RH)) is used to convert α to "dry extinction coefficient" (α_{dry}) by a series of empirical formulas (Che et al., 2007). $PM_{+\infty, j}$ ($\mu g \cdot m^{-3}$) can be retrieved individually from aerosol extinction coefficients for the seven aerosol types using Eq. (5). Then applying the bimodal lognormal size distributions of the CALIPSO aerosol models (Omar et al., 2009), the proportions of PM_{10} and $PM_{2.5}$ in $PM_{+\infty}$ for each aerosol type ($C_{i, j}$) can be determined using Eq. (8) and (9). Finally, both $PM_{10, j}$ and $PM_{2.5, j}$ of seven types of aerosol can be calculated. In this paper, we assume that the $C_{i, j}$ of the same aerosol in different regions is the same. In future work, we will discuss the $C_{i, j}$ difference of each aerosol in different regions in detail to modify our retrieval method. Finally, the lookup table for the key parameters of the retrieval method was summarized in Table 1. And the schematic diagram of the retrieval method was shown in Fig. 1.

$$\alpha_{dry} = \alpha \cdot f(RH) \tag{7}$$

$$C_{i,j} = \frac{\int_0^i dV/d \ln r}{\int_0^{+\infty} dV/d \ln r} dV/d \ln r \tag{8}$$

$$PM_{i,j} = PM_{+\infty,j} \cdot C_{i,j} \cdot f(RH) \tag{9}$$
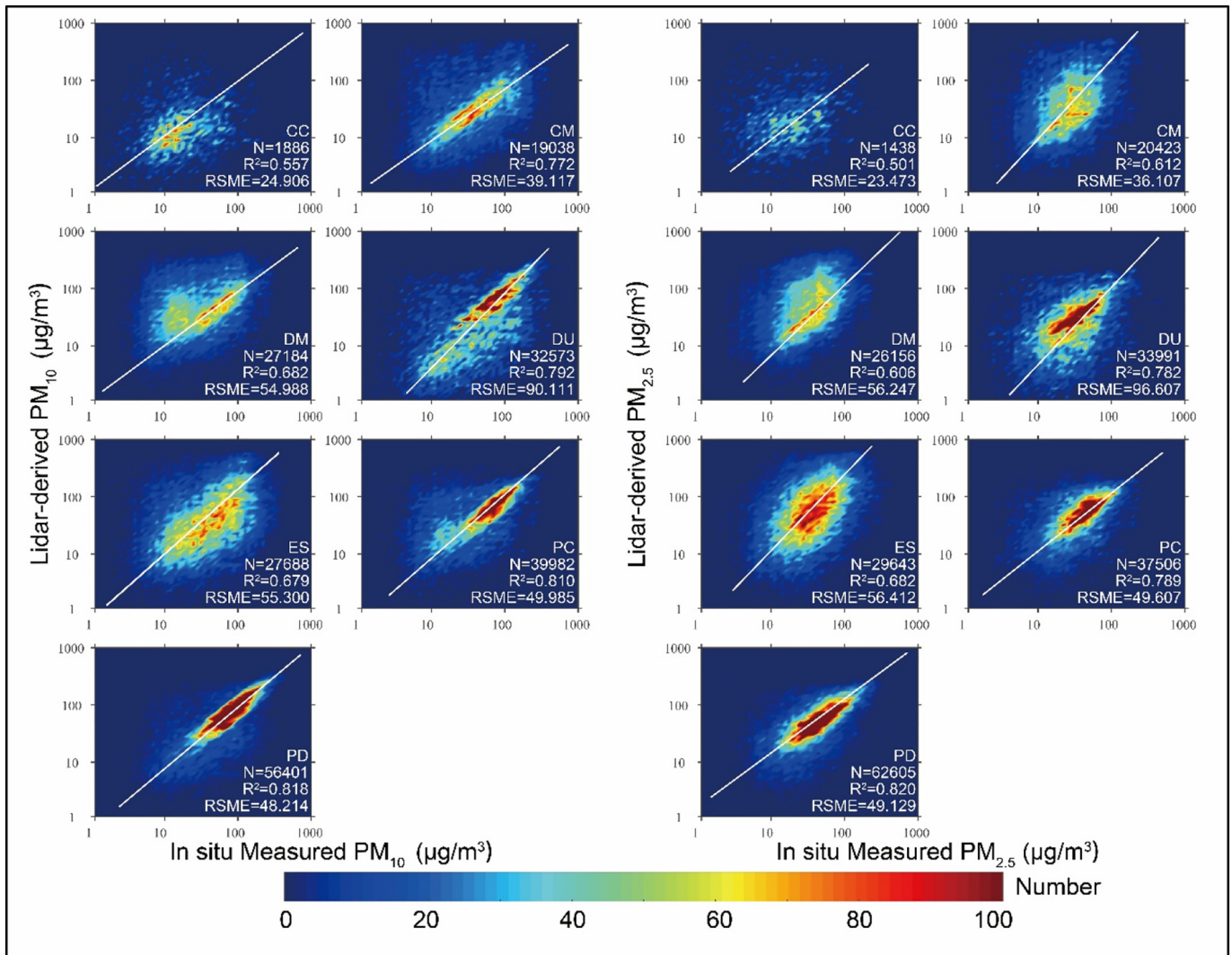
Fig. 3. Same as Fig. 2, but for seven types of aerosol individually.
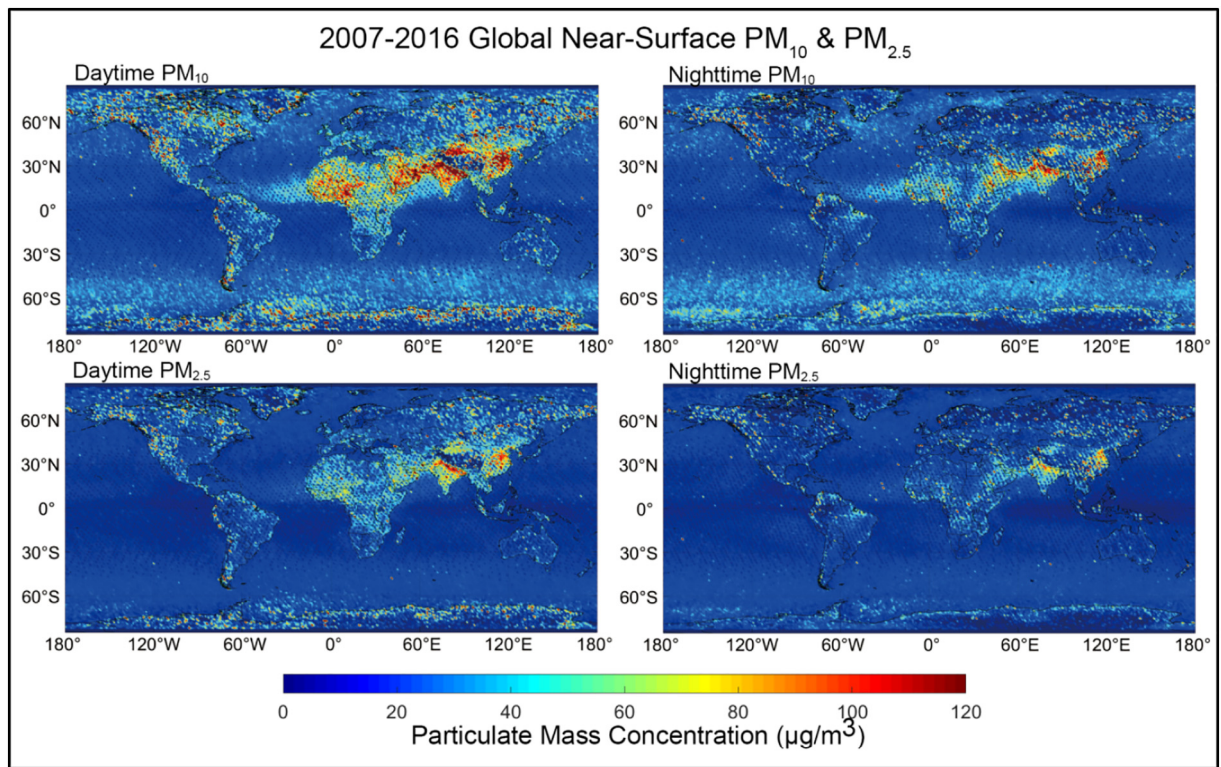
Fig. 4. Ten-year averaged global near-surface PM_{10} and $PM_{2.5}$ at daytime (left) and nighttime (right) from CALIPSO observation for 2007 to 2016. The size of the grid cells is $1° \times 1°$.

2.4. Validation

To validate the retrieval results, hourly PM_{10} and $PM_{2.5}$ mass concentrations from in situ measurements at 1602 ground monitoring sites throughout the world are used. Satellite data close to ground monitoring sites <5 km are selected to compare with the corresponding ground data. The number of profiles used to be considered valid for a comparison was 5 at least. Fig. 2 shows scatterplots of the hourly average in situ measured PM_{10} & $PM_{2.5}$ and lidar-derived PM_{10} & $PM_{2.5}$ from 2007 to 2016 in day and night respectively. The
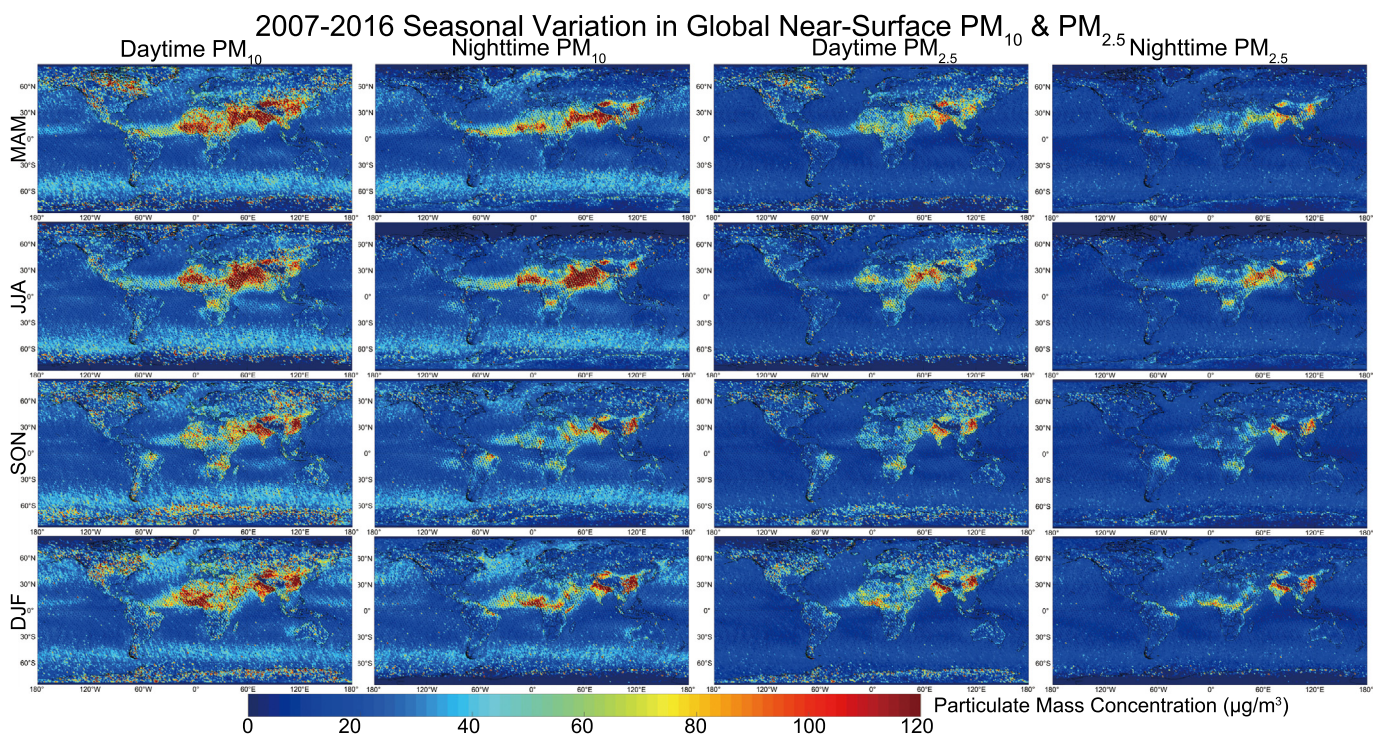
Fig. 5. Seasonal distributions of global near-surface PM_{10} and $PM_{2.5}$ at daytime and nighttime from CALIPSO observation for 2007 to 2016. The size of the grid cells is $1° \times 1°$.

results show that lidar-retrieved PM$_{10}$ & PM$_{2.5}$ good in agreement with in situ observations. The coefficient of variation (R^2) values are 0.763 and 0.729 for PM$_{10}$ and PM$_{2.5}$ in day, and are 0.732 and 0.683 for PM$_{10}$ and PM$_{2.5}$ at night. Moreover, lidar-derived PM$_{10}$ & PM$_{2.5}$ mass concentrations for the 7 aerosol types were compared individually with the hourly average in situ results, as shown in Fig. 3. It shows that mass concentrations of polluted dust were the best in among the 7 types of aerosol. Overall, the lidar-derived PM$_{10}$ showed higher credibility than the lidar-derived PM$_{2.5}$ when compared with in situ ground measurements.
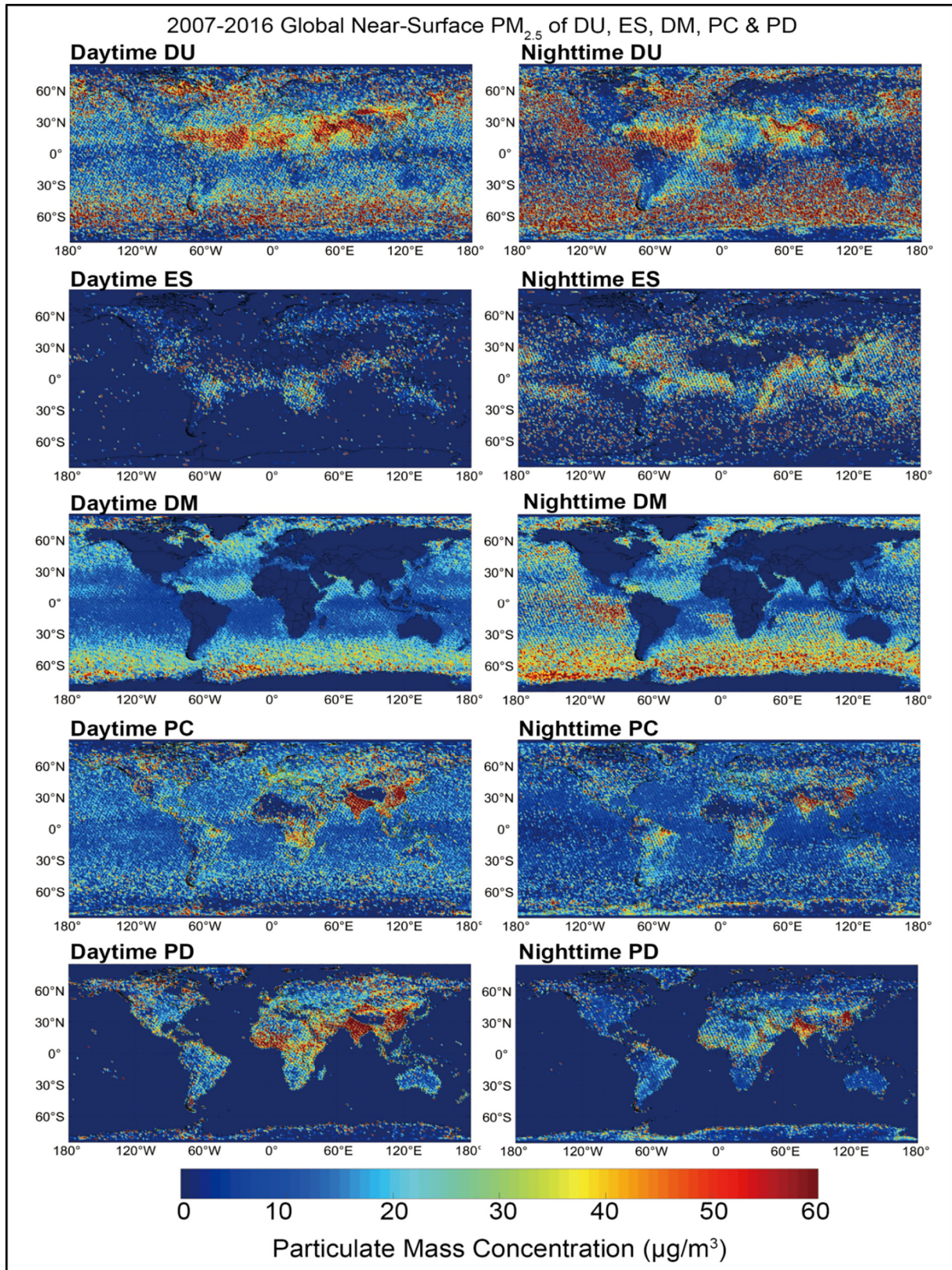
Fig. 6. Same as Fig. 4, but for pure dust (DU), elevated smoke (ES), dusty marine (DM), polluted continental (PC), and polluted dust (PD).

3. Results and discussion

Due to human activities and pollution emissions in different parts of the world (Wang et al., 2015; Zhong et al., 2017; Shi et al., 2018), PM mass concentrations during the day are higher than those at night (Pérez-Ramírez et al., 2012). PM_{10} is highly correlated with population in these highly polluted areas (Huang et al., 2014; Xie et al., 2015) during both day and night. Ten-year averaged global PM_{10} and $PM_{2.5}$ mass concentrations at daytime and nighttime for 2007–2016 are investigated as shown in Fig. 4. High PM_{10} mass concentrations can be found widely over dust source areas such as the Taklimakan Desert, Sahara Desert, Central Asia and the Middle East, and can reach $400\,\mu g \cdot m^{-3}$ during the day and $358\,\mu g \cdot m^{-3}$ at night. Increased dust uplift occurs during the day (Chen et al., 2018), causing higher PM_{10} above the surface than at night. Pasturage activities and dust uplifts led to increasing PM_{10} at daytime in Mongolia (Munkhtsetseg et al., 2016). Over the Antarctic Ocean from 30°S to 60°S, PM_{10} reached $55\,\mu g \cdot m^{-3}$ during the day and $50\,\mu g \cdot m^{-3}$ at night respectively. Substantial amounts of aerosols have been detected over the ocean in the Southern Hemisphere by in situ observations (Lu et al., 2016; Wilson et al., 2010). Sea spray aerosols were observed over the Antarctic Ocean (Aller et al., 2017; Wilson et al., 2010), possibly transported from South America and Antarctica. The results show that high PM_{10} and $PM_{2.5}$ was found at high latitudes of the Southern Hemisphere, which are same with observations from AERONET-Maritime Aerosol Network (Smirnov et al., 2009). Atmospheric nucleation events are globally common and are closely related to environmental humidity (Kulmala et al., 2013). A previous study (Hu et al., 2012) has shown that diffusion conditions at night are worse than those during the day, resulting in increased $PM_{2.5}$ concentrations. Diurnal variations of $PM_{2.5}$ over East Asia were extremely small, however for North America and Europe are remarkably higher. Moreover, the average $PM_{2.5}$ during the day ($48\,\mu g \cdot m^{-3}$) in the Southern Hemisphere is higher than that at night ($40\,\mu g \cdot m^{-3}$).

Seasonal distributions of global near-surface PM_{10} and $PM_{2.5}$ mass concentration retrieved from CALIPSO observations both in the day and at night are shown in Fig. 5. During spring in the Northern Hemisphere (MAM), the PM_{10} and $PM_{2.5}$ mass concentrations were higher than those in other seasons in the Taklimakan Desert and Sahara Desert due to the high frequency of dust uplifts, especially during the day. The Tibetan Plateau was affected by dust in spring and summer (Liu et al., 2008; Xu et al., 2018), leading to that PM was significantly higher during the day than that at night. During summer in the Northern Hemisphere (JJA), high PM_{10} concentrations occurred in northern India and the Middle East. Previous studies have confirmed long-range transportation of dust in the Middle East and northern India during summer; however, some MODIS results did not show high aerosol concentration in summer over the Middle East (Xie et al., 2013). The summer monsoon depression over the Bay of Bengal (Satheesh et al., 2009; Yoon and Chen, 2005) may have hindered the spread of pollution during both day and night, consequently PM_{10} and $PM_{2.5}$ concentrations increased during this period. In the high latitudes of the Northern Hemisphere the difference in PM between day and night was clear. More PC and PD appeared in summer, but less DU resulted in increased $PM_{2.5}$ and decreased PM_{10} (Kim et al., 2013).

During fall in the Northern Hemisphere (SON), the averages for both PM_{10} and $PM_{2.5}$ were higher than those in the other seasons in northern South America. In addition, the average summertime PM concentrations over the ocean in the Southern Hemisphere were the highest among the four seasons. This result suggests that some secondary aerosols may be produced under conditions of gradually increased ultraviolet radiation (Shrivastava et al., 2017). In the high latitudes of the Northern Hemisphere, differences in PM concentrations between day and night were obvious. DU appeared to be increased in fall, but the PC and PD concentrations were low; thus, PM_{10} was higher in fall than other seasons (Kim et al., 2013). Over the Taklimakan Desert the highest mass concentrations occurred in spring, but previous studies reported that PM_{10} and $PM_{2.5}$ in winter had the highest mass concentrations compared with the other three seasons (He and Huang, 2018; Ma et al., 2014). The probable main reason for these differences was overestimation of the results by passive remote sensing.

During winter in the Northern Hemisphere (DJF) a rapid increase in anthropogenic pollution emissions in Northern China, such as emissions
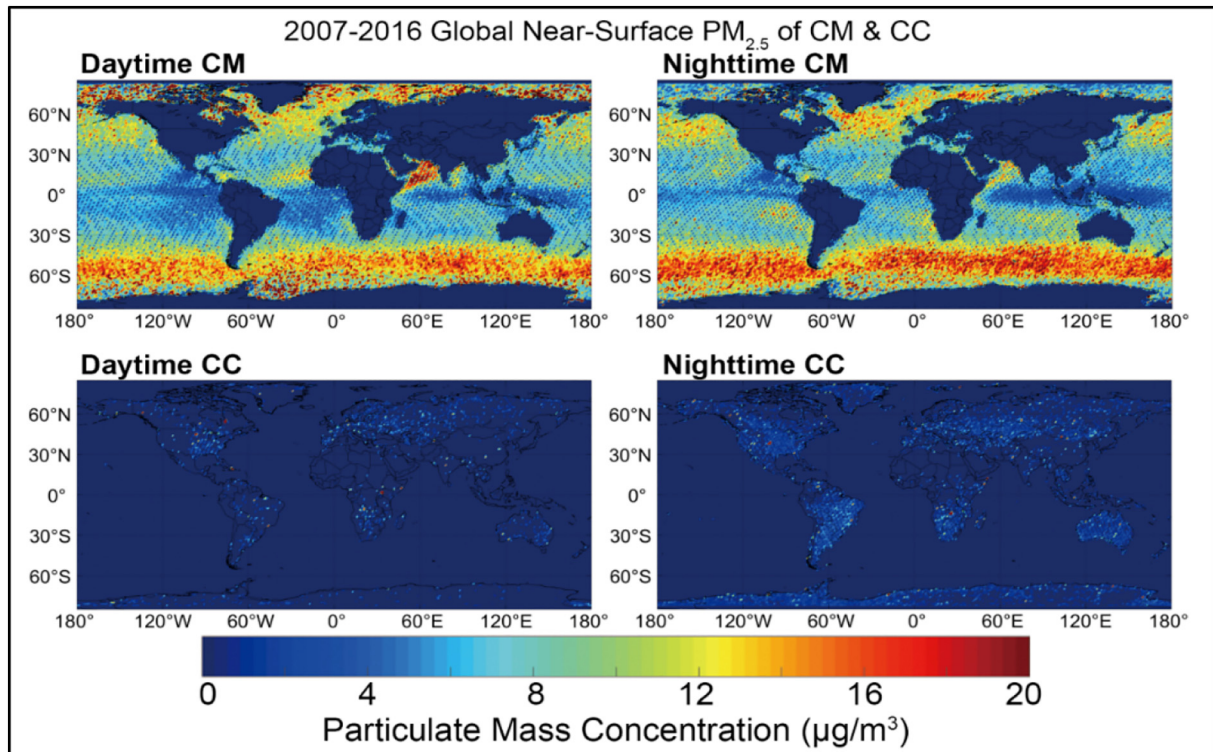
Fig. 7. Same as Fig. 6 but for clean marine (CM) and clean continental (CC).

from biomass burning or waste gas, resulted in an increased PM_{10} and $PM_{2.5}$which caused an increasing frequency of haze weather events (Chen et al., 2012; Zou et al., 2017). At the same time, the PM_{10} mass concentrations in northern India, especially near the south slope of the Tibetan Plateau, were higher than those in other seasons, as the population density was higher than that in Southern India. Spread of coal combustion pollution during the heating period is hindered at night. Some studies suggest that the interaction between aerosols and topography is the main reason for the increase in $PM_{2.5}$ in winter (Zhang et al., 2018).

Global distributions of individual $PM_{2.5}$ mass concentrations for seven types of aerosol are shown in Figs. 6 and 7. Over land, mass concentrations of all types of aerosols are higher during the day than at night; however, results over the ocean are different. $PM_{2.5}$ mass concentrations of CM, PC, PD and CC are higher during the day than at night, but for DM, ES and DU the results are the opposite. The types of aerosol that cause high mass concentrations in the Southern Hemisphere were DU

and DM. DU can lead to high mass concentrations over the Atlantic within latitudes 0 to 30°N. $PM_{2.5}$ with aerosol type of DU and DM is higher in nighttime than that in daytime over the Atlantic and the Antarctica. This phenomenon may attribute to the formation of secondary aerosols over the region.

To investigate the diurnal variations quantitatively, annual PM mass concentrations for four megacities are compared from 2007 to 2016, as shown in Fig. 8. The results show that annual PM_{10} mass concentrations in these four cities decreased gradually over the past decade. PM_{10} concentrations in Beijing and New Delhi were almost four times greater than those in New York and London. Furthermore, diurnal differences of PM_{10} concentrations in Beijing and New Delhi were much greater than those of $PM_{2.5}$ due to the effects of anthropogenic aerosol pollutants and haze (Chen et al., 2012; Liu et al., 2017). But for London and New York diurnal differences of PM_{10} was comparable with those of $PM_{2.5}$. We calculated the ratio of diurnal differences divided by mass concentration during the day. The results show that for Beijing the
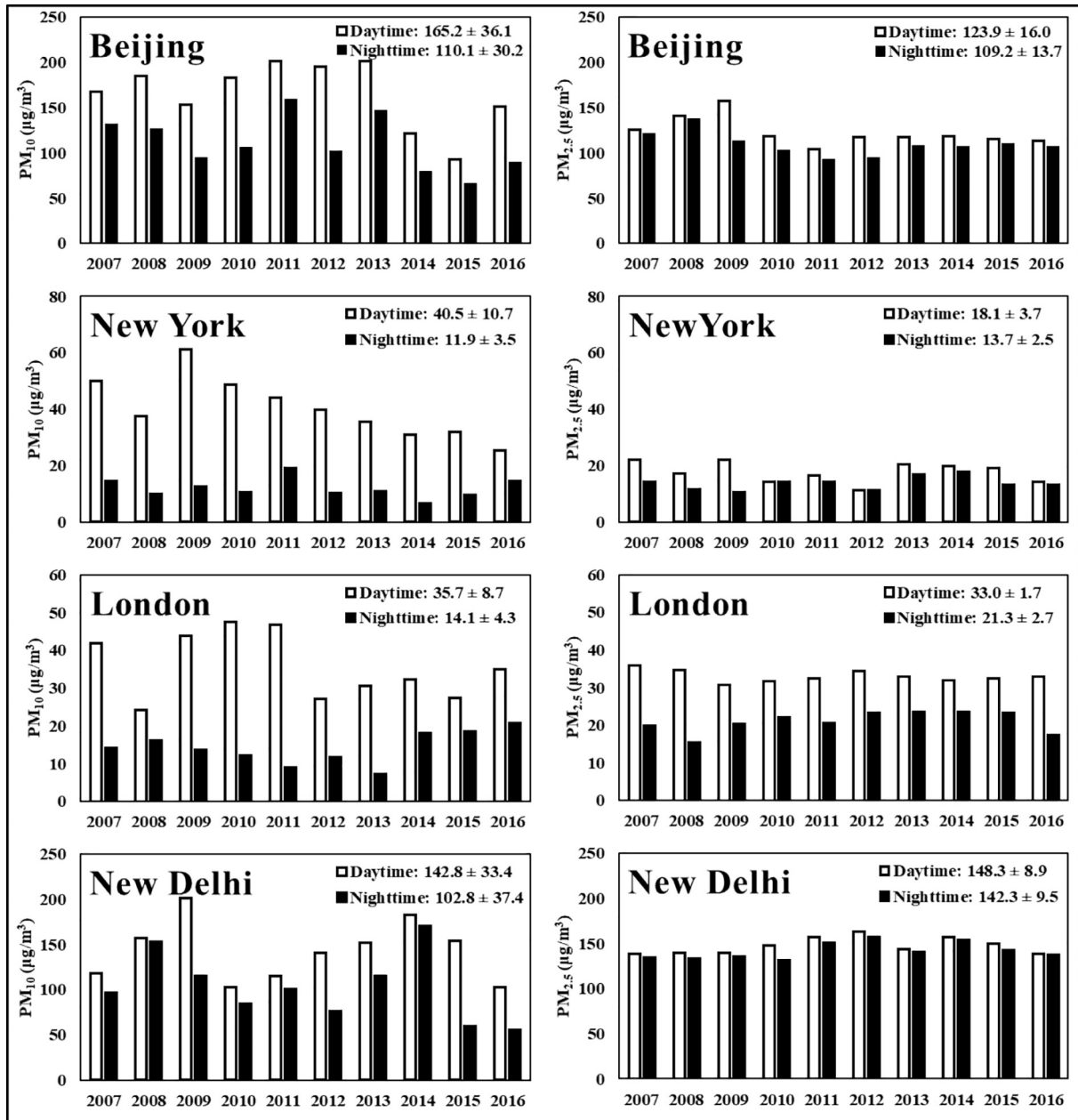
Fig. 8. Annual PM_{10} and $PM_{2.5}$ for four megacities during day (white) and night (black) from 2007 to 2016. Ten-year averaged PM mass concentrations with standard deviations for each city are shown in the upper-right corner of the panels.

annual mean $PM_{2.5}$ mass concentration at nighttime is only 11.31% less than those at daytime, however for London is 36.62%. Ten-year averaged PM_{10} concentrations in Beijing were higher than those in New Delhi, but for $PM_{2.5}$ concentrations are converse, indicating that aerosols in New Delhi mainly originate from human activities.

4. Conclusions

In this study, we estimated global PM_{10} and $PM_{2.5}$ mass concentrations both at daytime and nighttime from CALIPSO lidar observations. For the first time, ten-year global distributions of PM mass concentrations with high resolution both at daytime and nighttime were determined by use of spaceborne active remote sensing. The lidar-retrieved mass concentrations of PM_{10} and $PM_{2.5}$ are in good agreement with in situ observations from 1602 ground monitoring sites throughout the world. Over land, mass concentrations of typical seven types of aerosols are higher during the day than those at night. In summertime, high PM_{10} mass concentrations were found in northern India. Ten-year averaged PM_{10} mass concentration over the region are 200 $\mu g \cdot m^{-3}$ and 170 $\mu g \cdot m^{-3}$ for day and night respectively. Diurnal variations of PM_{10} and $PM_{2.5}$ mass concentrations over high population density regions such as East Asia and South Asia were small, but those were large for North America and others. And for Beijing the annual mean $PM_{2.5}$ mass concentration at nighttime is 11.31% less than those at daytime, however for London is 36.62%. This study provides a reliable long-term database of global particulate mass concentrations with high-resolution. The results not only can be used to validate global model simulations, but also evaluate aerosol impacts on climate, environment as well as ecosystem on a global scale.

CRediT authorship contribution statement

Xiaojun Ma: Formal analysis, Data curation, Writing - original draft, Writing - review & editing. **Zhongwei Huang:** Conceptualization, Methodology, Data curation, Writing - original draft, Writing - review & editing. **Siqi Qi:** Formal analysis. **Jianping Huang:** Conceptualization, Methodology, Data curation, Writing - original draft, Writing - review & editing. **Shuang Zhang:** Formal analysis. **Qingqing Dong:** Formal analysis. **Xin Wang:** Writing - review & editing.

Declaration of competing interest

The authors declare that they have no known competing financial interests or personal relationships that could have appeared to influence the work reported in this paper.

Appendix A. Supplementary data

Supplementary data to this article can be found online at https://doi.org/10.1016/j.scitotenv.2020.137699.

References

Aller, J.Y., Radway, J.A.C., Kilthau, W.P., Bothe, D.W., Wilson, T.W., Vaillancourt, R.D., Quinn, P.K., Coffman, D.J., Murray, B.J., Knopf, D.A., 2017. Size-resolved characterization of the polysaccharidic and proteinaceous components of sea spray aerosol. Atmos. Environ. 154, 331–347. https://doi.org/10.1016/j.atmosenv.2017.01.053.

Bi, J., Huang, J., Hu, Z., Holben, B., Guo, Z., 2014. Investigating the aerosol optical and radiative characteristics of heavy haze episodes in Beijing during January of 2013. Journal of Geophysical Research: Atmospheres 119 (16), 9884–9900. https://doi.org/10.1002/2014JD021757.

Che, H., Zhang, X., Li, Y., Zhou, Z., Qu, J.J., 2007. Horizontal visibility trends in China 1981-2005. Geophys. Res. Lett. 34, 1–5. https://doi.org/10.1029/2007GL031450.

Chen, B., Huang, J., Minnis, P., Hu, Y., Yi, Y., Liu, Z., Zhang, D., Wang, X., 2010. Detection of dust aerosol by combining CALIPSO active lidar and passive IIR measurements. Atmos. Chem. Phys. 10, 4241–4251. https://doi.org/10.5194/acp-10-4241-2010.

Chen, S., Yuan, T., Zhang, X., Zhang, G., Feng, T., Zhao, D., Zang, Z., Liao, S., Ma, X., Jiang, N., Zhang, J., Yang, F., Lu, H., 2018. Dust modeling over East Asia during the summer of 2010 using the WRF-Chem model. J. Quant. Spectrosc. Radiat. Transf. 213, 1–12. https://doi.org/10.1016/j.jqsrt.2018.04.013.

Chen, G., Li, S., Knibbs, L.D., Hamm, N.A.S., Cao, W., Li, T., Guo, J., Ren, H., Abramson, M.J., Guo, Y., 2018. A machine learning method to estimate PM2.5concentrations across China with remote sensing, meteorological and land use information. Sci. Total Environ. 636, 52–60. https://doi.org/10.1016/j.scitotenv.2018.04.251.

Chen, Y., Liu, Q., Geng, F., Zhang, H., Cai, C., Xu, T., Ma, X., Li, H., 2012. Vertical distribution of optical and micro-physical properties of ambient aerosols during dry haze periods in Shanghai. Atmos. Environ. 50. https://doi.org/10.1016/j.atmosenv.2012.01.002.

Donkelaar, A., Martin, R.V., Park, R.J., 2006. Estimating ground-level PM2.5 using aerosol optical depth determined from satellite remote sensing. J. Geophys. Res. Atmos. 111, 1–10. https://doi.org/10.1029/2005JD006996.

van Donkelaar, A., Martin, R.V., Brauer, M., Hsu, N.C., Kahn, R.A., Levy, R.C., Lyapustin, A., Sayer, A.M., Winker, D.M., 2016. Global estimates of fine particulate matter using a combined geophysical-statistical method with information from satellites, models, and monitors. Environ. Sci. Technol. 50, 3762–3772. https://doi.org/10.1021/acs.est.5b05833.

Fu, D., Xia, X., Duan, M., Zhang, X., Li, X., Wang, J., Liu, J., 2018. Mapping nighttime PM2.5from VIIRS DNB using a linear mixed-effect model. Atmos. Environ. 178, 214–222. https://doi.org/10.1016/j.atmosenv.2018.02.001.

Fu, Q., Thorsen, T.J., Su, J., Ge, J.M., Huang, J.P., 2009. Test of Mie-based single-scattering properties of non-spherical dust aerosols in radiative flux calculations. J. Quant. Spectrosc. Radiat. Transf. 110, 1640–1653. https://doi.org/10.1016/j.jqsrt.2009.03.010.

Geng, G., Zhang, Q., Martin, R.V., van Donkelaar, A., Huo, H., Che, H., Lin, J., He, K., 2015. Estimating long-term PM2.5concentrations in China using satellite-based aerosol optical depth and a chemical transport model. Remote Sens. Environ. 166, 262–270. https://doi.org/10.1016/j.rse.2015.05.016.

Ghotbi, S., Sotoudeheian, S., Arhami, M., 2016. Estimating urban ground-level PM10using MODIS 3km AOD product and meteorological parameters from WRF model. Atmos. Environ. 141, 333–346. https://doi.org/10.1016/j.atmosenv.2016.06.057.

He, Q., Huang, B., 2018. Satellite-based mapping of daily high-resolution ground PM2.5 in China via space-time regression modeling. Remote Sens. Environ. 206, 72–83. https://doi.org/10.1016/j.rse.2017.12.018.

Holben, B.N., Eck, T.F., Slutsker, I., Tanré, D., Buis, J.P., Setzer, A., Vermote, E., Reagan, J.A., Kaufman, Y.J., Nakajima, T., Lavenu, F., Jankowiak, I., Smirnov, A., 1998. AERONET - a federated instrument network and data archive for aerosol characterization. Remote Sens. Environ. 66, 1–16. https://doi.org/10.1016/S0034-4257(98)00031-5.

Holben, B.N., Tanré, D., Smirnov, A., Eck, T.F., Slutsker, I., Abuhassan, N., Newcomb, W.W., Schafer, J.S., Chatenet, B., Lavenu, F., Kaufman, Y.J., Vande Castle, J., Setzer, A., Markham, B., Clark, D., Frouin, R., Halthore, R., Karneli, A., O'Neill, N.T., Pietras, C., Pinker, R.T., Voss, K., Zibordi, G., 2001. An emerging ground-based aerosol climatology: aerosol optical depth from AERONET. J. Geophys. Res. Atmos. 106, 12067–12097. https://doi.org/10.1029/2001JD900014.

Hu, M., Peng, J., Sun, K., Yue, D., Guo, S., Wiedensohler, A., Wu, Z., 2012. Estimation of size-resolved ambient particle density based on the measurement of aerosol number, mass, and chemical size distributions in the winter in Beijing. Environ. Sci. Technol. 46, 9941–9947. https://doi.org/10.1021/es204073t.

Hu, X., Waller, L.A., Lyapustin, A., Wang, Y., Al-Hamdan, M.Z., Crosson, W.L., Estes, M.G., Estes, S.M., Quattrochi, D.A., Puttaswamy, S.J., Liu, Y., 2014. Estimating ground-level PM2.5 concentrations in the southeastern United States using MAIAC AOD retrievals and a two-stage model. Remote Sens. Environ. 140, 220–232. https://doi.org/10.1016/j.rse.2013.08.032.

Huang, J., Minnis, P., Yi, Y., Tang, Q., Wang, X., Hu, Y., Liu, Z., Ayers, K., Trepte, C., Winker, D., 2007. Summer dust aerosols detected from CALIPSO over the Tibetan plateau. Geophys. Res. Lett. 34, L18805. https://doi.org/10.1029/2007GL029938.

Huang, J., Minnis, P., Chen, B., Huang, Z., Liu, Z., Zhao, Q., Yi, Y., Ayers, J.K., 2008. Long-range transport and vertical structure of Asian dust from CALIPSO and surface measurements during PACDEX. Journal of Geophysical Research: Atmospheres 113, D23212. https://doi.org/10.1029/2008JD010620.

Huang, J., Wang, T., Wang, W., Li, Z., Yan, H., 2014. Climate effects of dust aerosols over East Asian arid and semiarid regions. J. Geophys. Res. Atmos. 119, 1–8. https://doi.org/10.1002/2014JD021796.

Huang, J., Liu, J., Chen, B., Nasiri, S.L., 2015b. Detection of anthropogenic dust using CALIPSO lidar measurements. Atmos. Chem. Phys. 15, 11653–11665. https://doi.org/10.5194/acp-15-11653-2015.

Huang, Z., Huang, J., Bi, J., Wang, G., Wang, W., Fu, Q., Li, Z., Tsay, S.-C., Shi, J., 2010. Dust aerosol vertical structure measurements using three MPL lidars during 2008 China-U.S. joint dust field experiment. J. Geophys. Res. 115, D00K15. https://doi.org/10.1029/2009JD013273.

Huang, Z., Huang, J., Hayasaka, T., Wang, S., Zhou, T., Jin, H., 2015a. Short-cut transport path for Asian dust directly to the Arctic: a case study. Environ. Res. Lett. 10, 114018. https://doi.org/10.1088/1748-9326/10/11/114018.

Huang, Z., Nee, J.B., Chiang, C.W., Zhang, S., Jin, H., Wang, W., Zhou, T., 2018. Real-time observations of dust-cloud interactions based on polarization and Raman lidar measurements. Remote Sens. 10, 1–15. https://doi.org/10.3390/rs10071017.

Huang, Z., Qi, S., Zhou, T., Dong, Q., Ma, X., Zhang, S., Bi, J., Shi, J., 2020. Investigation of aerosol absorption with dual-polarization lidar observations. Opt. Express 28, 7028–7035. https://doi.org/10.1364/OE.390475.

Intergovernmental Panel on Climate Change, 2014. Climate Change 2014: Synthesis Report; Chapter Observed Changes and their Causes.

Just, A.C., Wright, R.O., Schwartz, J., Coull, B.A., Baccarelli, A.A., Tellez-Rojo, M.M., Moody, E., Wang, Y., Lyapustin, A., Kloog, I., 2015. Using high-resolution satellite aerosol optical depth to estimate daily PM2.5 geographical distribution in Mexico City. Environ. Sci. Technol. 49, 8576–8584. https://doi.org/10.1021/acs.est.5b00859.

Kampa, M., Castanas, E., 2008. Human health effects of air pollution. Environ. Pollut. 151, 362–367. https://doi.org/10.1016/j.envpol.2007.06.012.

Kar, J., Vaughan, M.A., Lee, K.P., Tackett, J.L., Avery, M.A., Garnier, A., Getzewich, B.J., Hunt, W.H., Josset, D., Liu, Z., Lucker, P.L., Magill, B., Omar, A.H., Pelon, J., Rogers, R.R., Toth, T.D., Trepte, C.R., Vernier, J.P., Winker, D.M., Young, S.A., 2018. CALIPSO lidar calibration at 532 nm: version 4 nighttime algorithm. Atmos. Meas. Tech. 11, 1459–1479. https://doi.org/10.5194/amt-11-1459-2018.

Kato, S., Loeb, N.G., Rose, F.G., Doelling, D.R., Rutan, D.A., Caldwell, T.E., Yu, L., Weller, R.A., 2013. Surface irradiances consistent with CERES-derived top-of-atmosphere shortwave and longwave irradiances. J. Clim. 26, 2719–2740. https://doi.org/10.1175/JCLI-D-12-00436.1.

Kim, M.H., Kim, S.W., Yoon, S.C., Omar, A.H., 2013. Comparison of aerosol optical depth between CALIOP and MODIS-aqua for CALIOP aerosol subtypes over the ocean. J. Geophys. Res. Atmos. 118, 13241–13252. https://doi.org/10.1002/2013JD019527.

Kim, M.-H., Omar, A.H., Tackett, J.L., Vaughan, M.A., Winker, D.M., Trepte, C.R., Hu, Y., Liu, Z., Poole, L.R., Pitts, M.C., Kar, J., Magill, B.E., 2018. The CALIPSO version 4 automated aerosol classification and lidar ratio selection algorithm. Atmos. Meas. Tech. 11, 6107–6135. https://doi.org/10.5194/amt-11-6107-2018.

Koelemeijer, R.B.A., Homan, C.D., Matthijsen, J., 2006. Comparison of spatial and temporal variations of aerosol optical thickness and particulate matter over Europe. Atmos. Environ. 40, 5304–5315. https://doi.org/10.1016/j.atmosenv.2006.04.044.

Kulmala, M., Kontkanen, J., Junninen, H., Lehtipalo, K., Manninen, H.E., Nieminen, T., Petäjä, T., Sipilä, M., Schobesberger, S., Rantala, P., Franchin, A., Jokinen, T., Järvinen, E., Äijälä, M., Kangasluoma, J., Hakala, J., Aalto, P.P., Paasonen, P., Mikkilä, J., Vanhanen, J., Aalto, J., Hakola, H., Makkonen, U., Ruuskanen, T., Mauldin, R.L., Duplissy, J., Vehkamäki, H., Bäck, J., Kortelainen, A., Riipinen, I., Kurtén, T., Johnston, M.V., Smith, J.N., Ehn, M., Mentel, T.F., Lehtinen, K.E.J., Laaksonen, A., Kerminen, V.M., Worsnop, D.R., 2013. Direct observations of atmospheric aerosol nucleation. Science 339, 943–946. https://doi.org/10.1126/science.1227385.

Kumar, A., Singh, N., Anshumali, Solanki, R., 2018. Evaluation and utilization of MODIS and CALIPSO aerosol retrievals over a complex terrain in Himalaya. Remote Sens. Environ. 206, 139–155. https://doi.org/10.1016/j.rse.2017.12.019.

Laven, P., 2004. Simulation of rainbows, coronas and glories using Mie theory and the Debye series. J. Quant. Spectrosc. Radiat. Transf. 89, 257–269. https://doi.org/10.1016/j.jqsrt.2004.05.026.

Li, J., Huang, J., Stamnes, K., Wang, T., Lv, Q., Jin, H., 2015a. A global survey of cloud overlap based on CALIPSO and CloudSat measurements. Atmos. Chem. Phys. 15, 519–536. https://doi.org/10.5194/acp-15-519-2015.

Li, S., Joseph, E., Min, Q., 2016. Remote sensing of ground-level PM2.5 combining AOD and backscattering profile. Remote Sens. Environ. 183, 120–128. https://doi.org/10.1016/j.rse.2016.05.025.

Li, Y., Lin, C., Lau, A.K.H., Liao, C., Zhang, Y., Zeng, W., Li, C., Fung, J.C.H., Tse, T.K.T., 2015b. Assessing long-term trend of particulate matter pollution in the Pearl River Delta region using satellite remote sensing. Environ. Sci. Technol. 49, 11670–11678. https://doi.org/10.1021/acs.est.5b02776.

Lin, C., Li, Y., Yuan, Z., Lau, A.K.H., Li, C., Fung, J.C.H., 2015. Using satellite remote sensing data to estimate the high-resolution distribution of ground-level PM2.5. Remote Sens. Environ. 156, 117–128. https://doi.org/10.1016/j.rse.2014.09.015.

Liu, Q., He, Q., Fang, S., Guang, Y., Ma, C., Chen, Y., Kang, Y., Pan, H., Zhang, H., Yao, Y., 2017. Vertical distribution of ambient aerosol extinctive properties during haze and haze-free periods based on the micro-pulse Lidar observation in Shanghai. Sci. Total Environ. 574, 1502–1511. https://doi.org/10.1016/j.scitotenv.2016.08.152.

Liu, Z., Liu, D., Huang, J., Vaughan, M., Uno, I., Sugimoto, N., Kittaka, C., Trepte, C., Wang, Z., Hostetler, C., Winker, D., 2008. Airborne dust distributions over the Tibetan plateau and surrounding areas derived from the first year of CALIPSO lidar observations. Atmos. Chem. Phys. 8, 5045–5060. https://doi.org/10.5194/acp-8-5045-2008.

Liu, Z., Kar, J., Zeng, S., Tackett, J., Vaughan, M., Avery, M., Pelon, J., Getzewich, B., Lee, K., Magill, B., Omar, A., Lucker, P., Trepte, C., Winker, D., 2018. Discriminating between clouds and aerosols in the CALIOP version 4.1 data products. Atmos. Meas. Tech. 12, 703–734. https://doi.org/10.5194/amt-12-703-2019.

Lock, J.A., Laven, P., Adam, J.A., 2014. Scattering of a plane electromagnetic wave by a generalized Luneburg sphere-part 1: ray scattering. J. Quant. Spectrosc. Radiat. Transf. 162, 154–163. https://doi.org/10.1016/j.jqsrt.2015.02.013.

Lu, X., Hu, Y., Pelon, J., Trepte, C., Liu, K., Rodier, S., Zeng, S., Lucker, P., Verhappen, R., Wilson, J., Audouy, C., Ferrier, C., Haouchine, S., Hunt, B., Getzewich, B., 2016. Retrieval of ocean subsurface particulate backscattering coefficient from space-borne CALIOP lidar measurements. Opt. Express 24, 29001–29008. https://doi.org/10.1364/OE.24.029001.

Ma, X., Bartlett, K., Harmon, K., Yu, F., 2013. Comparison of AOD between CALIPSO and MODIS: significant differences over major dust and biomass burning regions. Atmos. Meas. Tech. 6, 2391–2401. https://doi.org/10.5194/amt-6-2391-2013.

Ma, Z., Hu, X., Huang, L., Bi, J., Liu, Y., 2014. Estimating ground-level PM2.5 in China using satellite remote sensing. Environ. Sci. Technol. 48, 7436–7444. https://doi.org/10.1021/es5009399.

Munkhtseteg, E., Shinoda, M., Gillies, J.A., Kimura, R., King, J., Nikolich, G., 2016. Relationships between soil moisture and dust emissions in a bare sandy soil of Mongolia. Particuology 28, 131–137. https://doi.org/10.1016/j.partic.2016.03.001.

Omar, A., Tackett, J., Kim, M.-H., Vaughan, M., Kar, J., Trepte, C., Winker, D., 2018. Enhancements to the caliop aerosol subtyping and lidar ratio selection algorithms for level II version 4. EPJ Web Conf 176, 02006. https://doi.org/10.1051/epjconf/201817602006.

Omar, A.H., Winker, D.M., Kittaka, C., Vaughan, M.A., Liu, Z., Hu, Y., Trepte, C.R., Rogers, R.R., Ferrare, R.A., Lee, K.P., Kuehn, R.E., Hostetler, C.A., 2009. The CALIPSO automated aerosol classification and lidar ratio selection algorithm. J. Atmos. Ocean. Technol. https://doi.org/10.1175/2009JTECHA1231.1.

Pérez-Ramírez, D., Lyamani, H., Olmo, F.J., Whiteman, D.N., Alados-Arboledas, L., 2012. Columnar aerosol properties from sun-and-star photometry: statistical comparisons and day-to-night dynamic. Atmos. Chem. Phys. 12, 9719–9738. https://doi.org/10.5194/acp-12-9719-2012.

Satheesh, S.K., Vinoj, V., Suresh Babu, S., Krishna Moorthy, K.S., Nair, V., 2009. Vertical distribution of aerosols over the east coast of India inferred from airborne LIDAR measurements. Ann. Geophys. 27, 4157–4169. https://doi.org/10.5194/angeo-27-4157-2009.

Shen, H., Li, T., Yuan, Q., Zhang, L., 2018. Estimating regional ground-level PM 2.5 directly from satellite top-of-atmosphere reflectance using deep belief networks. J. Geophys. Res. Atmos. 123, 13,875–13,886. https://doi.org/10.1029/2018JD028759.

Shi, Y., Matsunaga, T., Yamaguchi, Y., Zhao, A., Li, Z., Gu, X., 2018. Long-term trends and spatial patterns of PM2.5-induced premature mortality in south and Southeast Asia from 1999 to 2014. Sci. Total Environ. 631–632, 1504–1514. https://doi.org/10.1016/j.scitotenv.2018.03.146.

Shrivastava, M., Cappa, C.D., Fan, J., Goldstein, A.H., Guenther, A.B., Jimenez, J.L., Kuang, C., Laskin, A., Martin, S.T., Ng, N.L., Petaja, T., Pierce, J.R., Rasch, P.J., Roldin, P., Seinfeld, J.H., Shilling, J., Smith, J.N., Thornton, J.A., Volkamer, R., Wang, J., Worsnop, D.R., Zaveri, R.A., Zelenyuk, A., Zhang, Q., 2017. Recent advances in understanding secondary organic aerosol: implications for global climate forcing. Rev. Geophys. 55, 509–559. https://doi.org/10.1002/2016RG000540.

Smirnov, A., Holben, B.N., Slutsker, I., Giles, D.M., McClain, C.R., Eck, T.F., Sakerin, S.M., Macke, A., Croot, P., Zibordi, G., Quinn, P.K., Sciare, J., Kinne, S., Harvcy, M., Smyth, T.J., Piketh, S., Zielinski, T., Proshutinsky, A., Goes, J.I., Nelson, N.B., Larouche, P., Radionov, V.F., Goloub, P., Krishna Moorthy, K., Matarrese, R., Robertson, E.J., Jourdin, F., 2009. Maritime aerosol network as a component of aerosol robotic network. J. Geophys. Res. Atmos. 114. https://doi.org/10.1029/2008JD011257.

Stubenrauch, C.J., Rossow, W.B., Kinne, S., Ackerman, S., Cesana, G., Chepfer, H., Di Girolamo, L., Getzewich, B., Guignard, A., Heidinger, A., Maddux, B.C., Menzel, W.P., Minnis, P., Pearl, C., Platnick, S., Poulsen, C., Riedi, J., Sun-Mack, S., Walther, A., Winker, D., Zeng, S., Zhao, G., 2013. ASSESSMENT OF GLOBAL CLOUD DATASETS FROM SATELLITES: project and database initiated by the GEWEX radiation panel. Bull. Am. Meteorol. Soc. 94, 1031–1049. https://doi.org/10.1175/BAMS-D-12-00117.1 130117123745009.

Su, J., Huang, J., Fu, Q., Minnis, P., Ge, J., Bi, J., 2008. Estimation of Asian dust aerosol effect on cloud radiation forcing using Fu-Liou radiative model and CERES measurements. Atmos. Chem. Phys. 8, 2061–2084. https://doi.org/10.5194/acpd-8-2061-2008.

Sun, W., Baize, R.R., Videen, G., Hu, Y., Fu, Q., 2015. A method to retrieve super-thin cloud optical depth over ocean background with polarized sunlight. Atmos. Chem. Phys. 15, 11909–11918. https://doi.org/10.5194/acp-15-11909-2015.

Tao, Z., Wang, Z., Yang, S., Shan, H., Ma, X., Zhang, H., Zhao, S., Liu, D., Xie, C., Wang, Y., 2016. Profiling the PM 2.5 mass concentration vertical distribution in the boundary layer. Atmos. Meas. Tech. 9, 1369–1376. https://doi.org/10.5194/amt-9-1369-2016.

Toth, T.D., Zhang, J., Reid, J.S., Vaughan, M.A., 2018. A bulk-mass-modeling-based method for retrieving particulate matter pollution using CALIOP observations. Atmos. Meas. Tech. 12, 1739–1754. https://doi.org/10.5194/amt-12-1739-2019.

Wang, F., Guo, Z., Lin, T., Hu, L., Chen, Y., Zhu, Y., 2015. Characterization of carbonaceous aerosols over the East China Sea: the impact of the east Asian continental outflow. Atmos. Environ. 110, 163–173. https://doi.org/10.1016/j.atmosenv.2015.03.059.

Wang, J., Aegerter, C., Xu, X., Szykman, J.J., 2016. Potential application of VIIRS day/night band for monitoring nighttime surface PM2.5 air quality from space. Atmos. Environ. 124, 55–63. https://doi.org/10.1016/j.atmosenv.2015.11.013.

Wang, Z., Chen, L., Tao, J., Zhang, Y., Su, L., 2010a. Satellite-based estimation of regional particulate matter (PM) in Beijing using vertical-and-RH correcting method. Remote Sens. Environ. 114, 50–63. https://doi.org/10.1016/j.rse.2009.08.009.

Wang, W., Huang, J., Minnis, P., Hu, Y., Li, J., Huang, Z., Ayers, J.K., Wang, T., 2010. Dusty cloud properties and radiative forcing over dust source and downwind regions

derived from A-Train data during the Pacific Dust Experiment. J. Geophys. Res. Atmos. 115, D00H35. https://doi.org/10.1029/2010JD014109.

Wilson, D.I., Piketh, S.J., Smirnov, A., Holben, B.N., Kuyper, B., 2010. Aerosol optical properties over the South Atlantic and Southern Ocean during the 140th cruise of the M/VS.a. Agulhas. Atmos. Res. 98, 285–296. https://doi.org/10.1016/j.atmosres.2010.07.007.

Winker, D.M., Pelon, J., Coakley, J.A., Ackerman, S.A., Charlson, R.J., Colarco, P.R., Flamant, P., Fu, Q., Hoff, R.M., Kittaka, C., Kubar, T.L., Le Treut, H., McCormick, M.P., Mégie, G., Poole, L., Powell, K., Trepte, K., Vaughan, M.A., Wielicki, B.A., 2010. The Calipso Mission: a global 3D view of aerosols and clouds. Bull. Am. Meteorol. Soc. 91, 1211–1229. https://doi.org/10.1175/2010BAMS3009.1.

Xie, D., Cheng, T., Zhang, W., Yu, J., Li, X., Gong, H., 2013. Aerosol type over east Asian retrieval using total and polarized remote sensing. J. Quant. Spectrosc. Radiat. Transf. 129, 15–30. https://doi.org/10.1109/AFGR.1998.670992.

Xie, Y., Wang, Y., Zhang, K., Dong, W., Lv, B., Bai, Y., 2015. Daily estimation of ground-level PM2.5 concentrations over Beijing using 3 km resolution MODIS AOD. Environ. Sci. Technol. 49, 12280–12288. https://doi.org/10.1021/acs.est.5b01413.

Xu, C., Ma, Y., Yang, K., You, C., 2018. Tibetan plateau impacts on global dust transport in the upper troposphere. J. Clim. 31, 4745–4756. https://doi.org/10.1175/JCLI-D-17-0313.1.

Yang, T., Wang, Z., Zhang, W., Gbaguidi, A., Sugimoto, N., Wang, X., Matsui, I., Sun, Y., 2017. Technical note: boundary layer height determination from lidar for improving air pollution episode modeling: development of new algorithm and evaluation. Atmos. Chem. Phys. 17, 6215–6225. https://doi.org/10.5194/acp-17-6215-2017.

Yoon, J.H., Chen, T.C., 2005. Water vapor budget of the Indian monsoon depression. Tellus Ser. A Dyn. Meteorol. Oceanogr. 57, 770–782. https://doi.org/10.1111/j.1600-0870.2005.00145.x.

Zhang, Xin, Zhang, Q., Hong, C., Zheng, Y., Geng, G., Tong, D., Zhang, Y., Zhang, Xiaoye, 2018. Enhancement of PM2.5 concentrations by aerosol-meteorology interactions over China. J. Geophys. Res. Atmos. 123, 1179–1194. https://doi.org/10.1002/2017JD027524.

Zhong, Q., Huang, Y., Shen, H., Chen, Y., Chen, H., Huang, T., Zeng, E.Y., Tao, S., 2017. Global estimates of carbon monoxide emissions from 1960 to 2013. Environ. Sci. Pollut. Res. 24, 864–873. https://doi.org/10.1007/s11356-016-7896-2.

Zou, Y., Wang, Y., Zhang, Y., Koo, J.H., 2017. Arctic Sea ice, Eurasia snow, and extreme winter haze in China. Sci. Adv. 3, e1602751. https://doi.org/10.1126/sciadv.1602751.